3,5-Dianilino Substituted Difluoroboron Dipyrromethene: Synthesis, Spectroscopy, Photophysics, Crystal Structure, Electrochemistry, and Quantum-Chemical Calculations†

15 AUTHORS, INCLUDING:

Wim Dehaen
University of Leuven
568 PUBLICATIONS **9,258** CITATIONS

SEE PROFILE

David Beljonne
Université de Mons
355 PUBLICATIONS **15,262** CITATIONS

SEE PROFILE

Bernard Van Averbeke
Université de Mons
19 PUBLICATIONS **544** CITATIONS

SEE PROFILE

Mark Van der Auweraer
University of Leuven
333 PUBLICATIONS **8,461** CITATIONS

SEE PROFILE

3,5-Dianilino Substituted Difluoroboron Dipyrromethene: Synthesis, Spectroscopy, Photophysics, Crystal Structure, Electrochemistry, and Quantum-Chemical Calculations[†]

Wenwu Qin,[‡,§] Volker Leen,[§] Wim Dehaen,[§] Jie Cui,[‡] Chan Xu,[‡] Xiaoliang Tang,[‡] Weisheng Liu,[‡] Taoufik Rohand,[§] David Beljonne,[‖] Bernard Van Averbeke,[‖] John N. Clifford,[§] Kris Driesen,[§] Koen Binnemans,[§] Mark Van der Auweraer,[§] and Noël Boens*,[§]

College of Chemistry and Chemical Engineering, Lanzhou University, Lanzhou 730000, China, Department of Chemistry, Katholieke Universiteit Leuven, Celestijnenlaan 200f - bus 02404, 3001 Leuven, Belgium, and Laboratory for Chemistry of Novel Materials, University of Mons-Hainaut, Place du Parc 20, 7000 Mons, Belgium

4,4-Difluoro-3,5-bis(phenylamino)-8-(4-tolyl)-4-bora-3a,4a-diaza-*s*-indacene (**1**), a symmetric fluorescent difluoroboron dipyrromethene dye, has been synthesized by nucleophilic substitution of 3,5-dichloro-4,4-difluoro-8-(4-tolyl)-4-bora-3a,4a-diaza-*s*-indacene with aniline. The solvent-dependent spectroscopic and photophysical properties have been investigated by means of UV−vis spectrophotometry and steady-state and time-resolved fluorometry and are compared to those of the nonsymmetrically substituted 5-chloro-4,4-difluoro-3-phenylamino-8-(4-tolyl)-4-bora-3a,4a-diaza-*s*-indacene (**2**). A new, generalized treatment of the solvent effect, proposed by Catalán (*J. Phys. Chem. B* **2009**, *113*, 5951−5960) and based on a set of four mutually independent, empirical scales (dipolarity, polarizability, acidity, and basicity of the medium) is the most appropriate for describing the solvatochromic shifts of the UV−vis absorption and fluorescence emission of **1** and **2**. In contrast to the nonsymmetric compound **2**, the symmetric dye **1** has higher fluorescence quantum yields (0.45−0.86) and longer fluorescence lifetimes (3.36−4.03 ns) in all solvents studied and its emission maxima are shifted bathochromically by ∼45 nm. Large differences are also evident in the redox electrochemistry of the two dyes, with the symmetric analogue **1** possessing a much lower oxidation potential (∼600 mV) than the nonsymmetric **2**. The absorption bandwidths and Stokes shifts of symmetric **1** are much smaller than those for nonsymmetric **2**. For both dyes, the value of the fluorescence rate constant, [$k_f = (1.7 \pm 0.3) \times 10^8$ s^{-1}], does not depend much on the solvent tested. X-ray diffraction analysis of **1** shows that the BODIPY core possesses a planar structure. Quantum-chemical calculations support the different photophysical behavior of the symmetric derivative **1** vis-à-vis the nonsymmetric **2**.

Introduction

Derivatives of 4,4-difluoro-4-bora-3a,4a-diaza-*s*-indacene[1,2] (better known under the commercial name "BODIPY" or difluoroboron dipyrromethene) have become popular fluorophores in numerous fields of modern materials and life sciences.[3] In recent years, a continually increasing number of research publications has focused on the syntheses, functionalization reactions, and spectroscopic/photophysical properties of these dyes.[4] The outstanding qualities of BODIPY consist of relatively high fluorescence quantum yields Φ_f (often approaching 1.0) and molar absorption coefficients ($\varepsilon > 50\,000$ L mol^{-1} cm^{-1}), narrow emission bandwidths with high peak intensities, excellent thermal and photochemical stability, good solubility, chemical robustness, negligible triplet-state formation, and excitation/emission spectra in the visible region. Moreover, it is rather straightforward to develop different BODIPY analogues with emission wavelengths tunable from 500 nm to over 700 nm, by attaching supplementary units at the pyrrole,[5] *meso*,[6−9] and *N-ortho* positions.[10−17] The spectroscopic/photophysical proper-

ties of several BODIPY dyes in solution have been studied by means of UV−vis absorption and fluorescence techniques.[9,14−18]

Recently, we described that 3,5-dichloroBODIPY[8,11,13] derivatives can be substituted with a wide range of oxygen, carbon, nitrogen, and sulfur centered nucleophiles[10,11,13] and that the reaction conditions can be adjusted to have either mono- or disubstitution.[11] Using this nucleophilic aromatic substitution reaction, Dilek and Bane prepared 3-hydrazinyl substituted BODIPY derivatives, which could be transformed into hydrazones.[19] It was shown that the nonsymmetric 3-hydrazinyl BODIPY dyes had larger absorption and emission bandwidths and Stokes shifts compared to classic difluoroboron dipyrromethenes.[9,18] Burgess et al. also utilized 3,5-dichloroBODIPY analogues as substrates to explore this S$_N$Ar displacement reaction.[20] Nonsymmetrically substituted BODIPY derivatives with an *N*-substituent at the 3-position had wider absorption and emission bands and larger Stokes shifts than symmetric BODIPY dyes. In a recent paper,[21] we described the crystal structure, electrochemistry, and spectroscopic and photophysical properties of the nonsymmetric 5-chloro-4,4-difluoro-3-phenylamino-8-(4-tolyl)-4-bora-3a,4a-diaza-*s*-indacene (**2**). In contrast to classic BODIPY derivatives, broader absorption and emission bands and larger Stokes shifts were also found for dye **2**.

In the present work, we describe the optimized synthetic conditions for the symmetric BODIPY dye 4,4-difluoro-3,5-bis(phenylamino)-8-(4-tolyl)-4-bora-3a,4a-diaza-*s*-indacene (**1**)
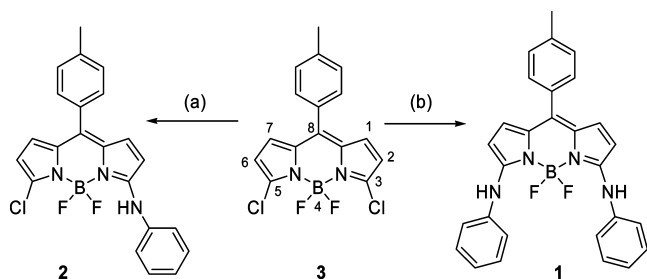

SCHEME 1: Synthesis of BODIPY Derivatives 1 and 2[a]

[a] Reaction conditions: (a) rt/acetonitrile + aniline/14 h (see ref 21); (b) 140 °C/aniline/4 h.

and investigate its spectroscopic and photophysical characteristics in several solvents by UV–vis spectrophotometry and steady-state and time-resolved fluorescence spectroscopy. These experiments allowed us to determine the wavelengths of the spectral maxima [λ_{abs}(max), λ_{ex}(max), λ_{em}(max)], the full width at half height of the maximum of the absorption (fwhm$_{abs}$) band, the Stokes shifts ($\Delta\bar{\nu}$), the fluorescence quantum yields (Φ_f), the fluorescence lifetimes (τ), and the rate constants of fluorescence (k_f) and nonradiative (k_{nr}) deactivation. We used single- and multiparameter expressions to describe the solvent effect on the positions of the spectral maxima and Stokes shifts of **1** and **2**. Furthermore, the electrochemical properties of **1** have been measured and are contrasted to those of **2**. In addition, the crystal structure of **1** has been determined. Finally, quantum-chemical calculations have been utilized to clarify the UV–vis spectra of **1**.

Experimental Section

Materials. All solvents for the spectroscopic measurements were of spectroscopic grade and were used without further purification. The chemicals for the synthesis were of reagent grade quality, procured from commercial sources, and used as received.

Syntheses. ***3,5-Dichloro-4,4-difluoro-8-(4-tolyl)-4-bora-3a,4a-diaza-s-indacene (3)*** is the starting compound for the synthesis of BODIPY derivatives **1** and **2** (Scheme 1) and was synthesized according to published procedures.[11,13] The detailed synthetic modus operandi for **2** has been described recently.[21] The optimized reactions conditions for **1** are given below.

4,4-Difluoro-3,5-bis(phenylamino)-8-(4-tolyl)-4-bora-3a,4a-diaza-s-indacene (1). The synthesis of **1** has been described before.[11] However, because this synthetic procedure is difficult to reproduce, we decided to optimize the reaction conditions of the synthesis of **1** (Table 1). First, we used the same solvent (acetonitrile) as described in ref 11 and changed the amount of aniline with respect to the starting compound **3**. It was found that long reaction times (days) were necessary to obtain moderate yields. The use of DMF as a solvent and/or microwave irradiation instead of conventional heating did not significantly improve the results. Finally, the breakthrough came when we decided to use aniline as solvent and nucleophile, producing high yields in a short time. The optimized synthetic procedure of **1** is given next.

To BODIPY derivative **3** (175 mg, 0.5 mmol) in a 10 mL round-bottom flask was added 4 mL of aniline (44 mmol, 88 equivs). The resulting mixture was stirred under argon until all the BODIPY was dissolved, after which the reaction mixture was heated at 140 °C for 4 h. After it was cooled down to room temperature, the reaction mixture was poured into diethyl ether (200 mL). The deep blue solution was then washed with water

TABLE 1: Optimization of the Reaction Conditions of the Synthesis of Compound 1

solvent	aniline/equiv	temp/°C	time	yield/%[a]
CH$_3$CN	4	reflux (81–82)[b]	14 days	42
CH$_3$CN	8	reflux (81–82)[b]	14 days	56
CH$_3$CN	16	reflux (81–82)[b]	10 days	57
DMF	8	120	48 h	26
DMF	8	150	8 h	11
CH$_3$CN	8	100 (MW)[c]	8 h	49
CH$_3$CN	8	120 (MW)[c]	8 h	57
DMF	8	120 (MW)[c]	4 h	[d]
aniline	[e]	140	4 h	81[f]
aniline	[e]	150	4 h	69

[a] Isolated yields (%) from a reaction with 0.1 mmol of BODIPY **3**. [b] Boiling point of acetonitrile. [c] Microwave reactions were irradiated at 150 W. [d] Complex reaction mixture with a small amount of product. [e] Aniline was used as solvent and nucleophile. [f] Isolated yield after optimization (see described procedure in text) for a reaction carried out with 0.5 mmol of **3**.

(3×200 mL), aqueous HCl (0.1 M, 2×200 mL), and brine (3×200 mL). The organic layer was dried over MgSO$_4$, filtered, and evaporated to dryness under reduced pressure. The solid residue was purified by flash-column chromatography [silica gel with dichloromethane + 1 vol % Et$_3$N] to yield 188 mg (81% yield) of a deep blue solid. Mp 210 °C. ^{1}H NMR (CDCl$_3$) δ 7.48 (s, broad, 2H, NH), 7.38 (d, 2H, $J = 8$ Hz), 7.34 (dd, apparent triplet, 4H, $J = 7.3$ and 7.8 Hz, m-anilino), 7.25 (d, 2H, $J = 8$ Hz), 7.22 (d, 4H, $J = 7.8$ Hz, o-anilino), 7.08 (t, 2H, $J = 7.3$ Hz, p-anilino), 6.67 (d, 2H, $J = 4.1$ Hz), 6.24 (d, 2H, $J = 4.1$ Hz), 2.43 (s, 3H, tolyl-CH$_3$). ^{13}C NMR (CDCl$_3$) δ 152.4, 139.7, 139.2, 133.3, 131.7, 130.4, 129.6, 129.3, 129.1, 129.0, 123.6, 120.1, 104.2, 21.5. LRMS (EI, 70 eV) m/z 464 (M$^+$ 100). HRMS: calcd for C$_{28}$H$_{23}$BF$_2$N$_4$ 464.1983, found 464.1991. IR: 2997, 1510, 1228 cm^{-1}.

^{1}H and ^{13}C NMR spectra were recorded at room temperature on a Bruker 600 instrument operating at a frequency of 600 MHz for ^{1}H and 150 MHz for ^{13}C. ^{1}H NMR spectra were referenced to tetramethylsilane (0.00 ppm) as an internal standard. Chemical shift multiplicities are reported as s = singlet, d = doublet, and t = triplet. ^{13}C NMR spectra were referenced to the CDCl$_3$ (77.67 ppm) signal. Mass spectra were recorded on a Hewlett-Packard 5989A mass spectrometer (EI mode and CI mode). High-resolution mass data were obtained with a KRATOS MS50TC instrument. Melting points were taken on an X-6 precise micro melting point cryoscope (Beijing Fukai Instrument Co.) and are uncorrected.

Crystal Structure Determination. Crystals of compound **1** with approximate dimensions of $0.26 \times 0.18 \times 0.152$ mm^3, suitable for X-ray diffraction, were obtained in good yield by slow evaporation of the mixed solvent (petroleum ether/dichloromethane) (3.5:1, v/v) in air over two weeks. The crystals belonged to the monoclinic space group $C2/c$ (number 15) with cell dimensions $a = 25.119(5)$ Å, $b = 13.313(2)$ Å, $c = 18.755(4)$ Å, $\beta = 118.811(14)°$, $V = 5495.5(17)$ Å^3, $Z = 8$, $\rho_{calc} = 1.328$ g cm^{-3}, $2\theta_{max} = 51.00°$, μ(Mo Kα) = 0.276 mm^{-1}. The data were collected at 294 ± 2 K using a Bruker Smart APEX II CCD diffractometer equipped with graphite-monochromated Mo Kα radiation ($\lambda = 0.71073$ Å). A total of 14561 reflections were measured, of which 5030 are unique. The structure was solved by direct methods. All non-hydrogen atoms were subjected to anisotropic refinement by full-matrix least-squares methods on F^2 data (goodness-of-fit on $F^2 = 1.003$) by using the software package SHELXS-97.[22] Hydrogen atoms were placed at calculated positions. Final R indices [$I > 2\sigma(I)$]

3,5-Dianilino Substituted Difluoroboron Dipyrromethene

J. Phys. Chem. C, Vol. 113, No. 27, 2009 **11733**

were $R_1 = 0.0697$, $wR_2 = 0.1286$; max/min residual electron densities were 0.530 and -0.424 eÅ^{-3}.

The crystal structure reported in this paper has been deposited at the Cambridge Crystallographic Data Centre and allocated the deposition number CCDC 721086. Copies of these data can be obtained free of charge on application to CCDC, 12 Union Road, Cambridge CB2 1EZ, U.K. (fax: +44(0)-1123-336033 or e-mail: deposit@ccdc.cam.ac.uk or www.ccdc.cam.ac.uk/conts/retrieving.html).

Cyclic Voltammetry. Electrochemical data were obtained using an Autolab PGSTAT12 potentiostat and a standard three-electrode cell (platinum working and counter electrodes and an Ag/AgCl reference) at a scan rate of 200 mV s^{-1}. The voltammograms were recorded at room temperature using a solution of 0.1 mol L^{-1} tetrabutylammonium hexafluorophosphate as the supporting electrolyte in dry dichloromethane. All solutions were purged with argon prior to measurement.

UV−Vis Steady-State Spectroscopy. UV−vis absorption spectra were determined on a Varian UV-Cary 100 spectrophotometer. Corrected fluorescence excitation and emission spectra were recorded on a Hitachi F-4500 spectrofluorometer. All absorption and fluorescence excitation/emission spectra were recorded at 20 °C using undegassed samples (degassing did not influence the fluorescence quantum yield, see below) in 1-cm quartz cells. For each dye in a specific solvent, three or four absorption, excitation, and emission spectra were measured as a function of dye concentration. Because the spectra are recorded digitally and the peaks are relatively narrow, the maxima can be determined not only from visual inspection but also via the analysis-calculus-integrate menu of the Origin software. The error on the wavelength of the maximum is commonly 1−2 nm. For the determination of the relative fluorescence quantum yields (Φ_f), only dilute solutions with an absorbance below 0.1 at the excitation wavelength λ_{ex} were used. Cresyl violet in methanol ($\lambda_{ex} = 546$ nm, $\Phi_f = 0.55$) was used as fluorescence standard.[23] The Φ_f values reported in this work are the averages of multiple (generally 3 or 4), fully independent measurements. The majority of the Φ_f determinations was done using undegassed samples. To check the influence of dissolved O$_2$ on Φ_f, a few samples, degassed via successive freeze−pump−thaw cycles, were measured. The obtained Φ_f values were within experimental error equal for aerated and degassed samples, in accordance with results for other BODIPY compounds.[9a] This supports the use of undegassed samples in the steady-state spectroscopic measurements. In all Φ_f determinations, correction for the solvent refractive index was applied.[24]

Time-Resolved Fluorescence Spectroscopy. Fluorescence decay traces of **1** were recorded at several emission wavelengths by the single-photon timing method.[25] Details of the instrumentation used and experimental procedures have been described elsewhere.[26] The samples were excited at 580 nm with a repetition rate of 8.10 MHz, using the frequency-doubled output from an OPO pumped by a picosecond Ti:sapphire laser. Fluorescence decay histograms were collected at the magic angle in 4096 channels with a time increment per channel of 1.8 ps, using 1-cm optical path length cells. The absorbance at the excitation wavelength was always below 0.1. All lifetime measurements were performed on samples that were degassed by consecutive freeze−pump−thaw cycles, to exclude the effect of dissolved oxygen on the fluorescence lifetimes. However, degassing did not have an influence: in the solvents used, the fluorescence lifetime of **1** was the same for aerated and degassed samples. Histograms of the instrument response function were recorded using a LUDOX scatterer. The full width at half height

of the maximum of the instrument response function was ∼60 ps. All measurements were done at 20 °C.

The fitting parameters were determined by minimizing the global, *reduced* chi-square function χ_g^2:

$$\chi_g^2 = \sum_l^q \sum_i w_{li}(y_{li}^o - y_{li}^c)^2/\nu \tag{1}$$

where the index l sums over q experiments and the index i sums over the appropriate channel limits for each individual experiment. y_{li}^o and y_{li}^c denote respectively the observed and calculated (i.e., fitted) values corresponding to the ith channel of the lth experiment, and w_{li} is the corresponding statistical weight. ν represents the number of degrees of freedom for the entire multidimensional fluorescence decay surface.

The statistical criteria for judging the quality of the fit included both graphical and numerical tests and have been described elsewhere.[25c,27] The decays were analyzed first individually by a (multi)exponential decay law in terms of decay times τ_i and their associated pre-exponential factors α_i. The final curve-fitting was done by global analysis in which decays recorded at six different emission wavelengths λ_{em} (610, 620, 630, 640, 660, and 680 nm) were described by a single-exponential decay function with linked lifetime τ and local (nonlinked) pre-exponentials α. The quality of the fit was assessed for each fluorescence decay trace separately as well as for the global fluorescence decay surface. All curve fittings reported here had χ^2 values below 1.1.

For the monoexponential fluorescence decays observed for **1**, the rate constants of fluorescence (k_f) and nonradiative (k_{nr}) deactivation can be calculated from the measured fluorescence quantum yield Φ_f and lifetime τ according to eq 2:

$$k_f = \Phi_f/\tau \tag{2a}$$

$$k_{nr} = (1 - \Phi_f)/\tau \tag{2b}$$

Computational Details. Molecular properties in the gas phase were obtained using semiempirical quantum-chemical methods. The ground-state (excited-state) geometry of molecule **1** was computed at the AM1 (AM1/CI) level.[28] These structures were subsequently used as input for electronic excited-state calculations performed at the INDO/SCI level.[29] The highest 40 occupied and lowest 40 unoccupied molecular orbitals were included in the SCI active space. On the basis of the optimized excited-state geometry, the gas-phase radiative decay rate constant of **1** was computed using eq 3 with $n = 1$:

$$k_f = \frac{8\pi^2 n^2 \bar{\nu}_{em}^3}{3\varepsilon_0 \hbar}|\mu|^2 \tag{3}$$

Here μ is the transition dipole moment (in C·m) from the lowest excited state to the ground state, and n stands for the refractive index of the medium. $\hbar = h/2\pi$ with h Planck's constant, $\bar{\nu}_{em}$ is the wavenumber of the emission maximum in m^{-1}, and ε_0 is the permittivity of vacuum. For comparison purposes, similar calculations have been done for **2**.
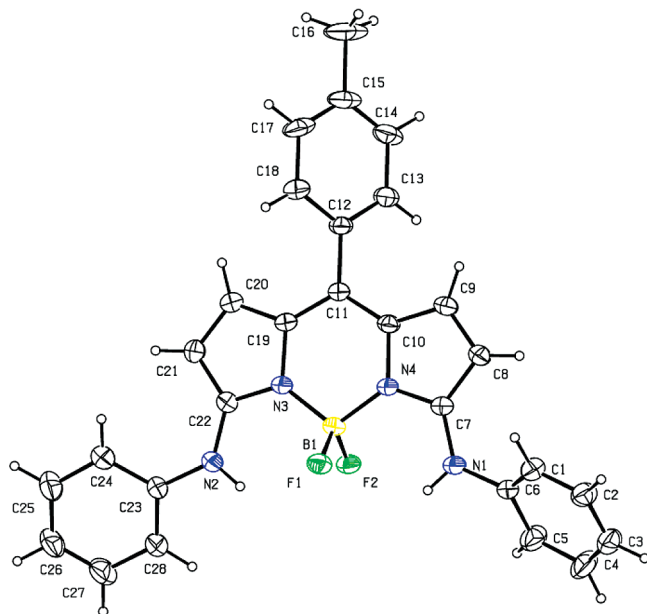
Figure 1. ORTEP representation of compound **1** with displacement ellipsoids at the 20% probability level. The cocrystallized CH$_2$Cl$_2$ solvent molecule close to C20 is omitted for clarity.

Results and Discussion

Dyes **1** and **2** were synthesized by an efficient S$_N$Ar reaction of compound **3**.[11] This synthetic methodology is particularly valuable for obtaining symmetrically (e.g., compound **1**) and nonsymmetrically substituted (e.g., compound **2**) boradiazaindacene dyes with substituents at the 3 (and 5) position(s) that are difficult to introduce otherwise.

Crystal Structure of 1. As shown in Figure 1, in the BODIPY ring system, the two planar pyrrole subunits and the boron atom constitute a plane for which the deviation of all non-hydrogen atoms is within the 0.012−0.070 Å range. The angle between the two pyrrole moieties is 4.27°, which is near the average 6.5° (range 0°−18.1°) found in the Cambridge Structural Database (CSD, updated until October 2008). The two fluorine atoms are equidistant above and under the plane of the pyrrole moieties, and the F−B−F plane is almost perpendicular (87.95°) to the plane of the BODIPY core. The phenyl ring at the *meso*-position makes an angle of 51.27° with the BODIPY plane, which is in the range of most BODIPY derivatives (40.3°−90°) but is smaller than the average value of 76.4° found in the CSD. In the solid state, the two aniline groups at the C7- and C22-position of **1** are inexactly enantiomorphous and the angles between the aniline rings and the BODIPY plane are 49.28° and 25.96°, respectively.

Four intramolecular hydrogen bonds are found between both NH groups and both fluorine atoms. Moreover, two compounds **1** are further linked to form a dimeric structure by intermolecular hydrogen bonds, N−H···F and C−H···F (Figure 2). Bond distances and angles for the hydrogen bonds are given in Table S1 (Supporting Information). The aggregation of **1** through a series of hydrogen bonds and π−π stacking interactions in the crystal cell is shown in Figure S1 (Supporting Information).

Electrochemistry. Figure 3 displays the cyclic voltammograms for compounds **1** and **2**, showing their one-electron oxidations. The oxidation potentials of the symmetric (**1**) and nonsymmetric (**2**) derivatives estimated from the midpoints of the forward and reverse peaks of the scan appear at ca. 0.54 and 1.14 V versus Ag/AgCl, respectively. For both compounds, upon scanning in the anodic direction, a precipitate can be
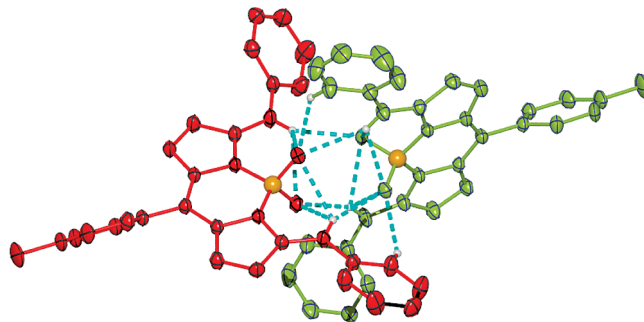

Figure 2. View of the dimeric structure of **1** linked by intramolecular and intermolecular hydrogen bonds. Hydrogen atoms, which do not form hydrogen bonds, are omitted for transparency. The two compounds are represented in a different color for clarity. Hydrogen bonds are denoted by turquoise broken lines.
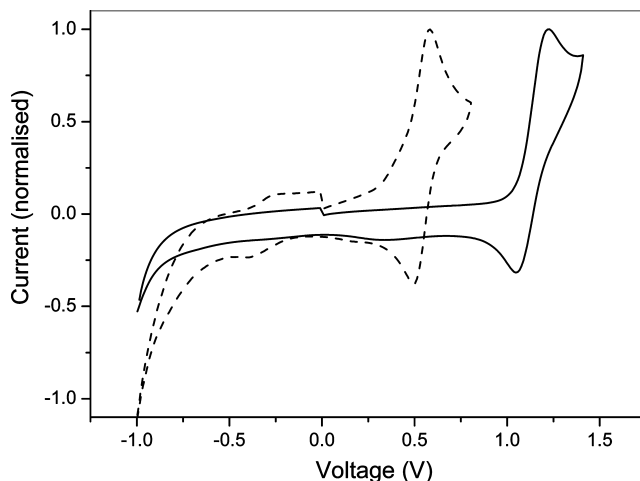

Figure 3. Cyclic voltammograms of the symmetric (**1**, - - -) and nonsymmetric (**2**, —) BODIPY dyes in degassed dichloromethane solutions containing 0.1 mol L^{-1} tetrabutylammonium hexafluorophosphate using a scan rate of 200 mV s^{-1}. The potentials are expressed versus an Ag/AgCl reference electrode.

clearly seen to form on the surface of the working electrode, which could be due to instability of the oxidized forms of **1** and **2**. This observation manifests itself in Figure 3 with the reverse scans displaying smaller current amplitudes than the forward scans. Upon moving to faster scan rates, this effect appears less pronounced; however, fully reversible forward and reverse scans are still not observed. We did not observe any reduction electrochemistry for either of these compounds and this could be because these redox potentials are beyond the accessible range of dichloromethane. However, even extending this range in the cathodic direction using solvents such as tetrahydrofuran and acetonitrile (solvents with a larger electrochemical window than that of dichloromethane) did not lead to the observation of a reduction wave. Considering that the optical band gap obtained from the absorption spectra is at least 2 eV (see below), this reduction potential must be around −1.5 eV versus Ag/AgCl. The large difference in oxidation potential between the two dyes is clearly due to the nature of their differing 5-substituents. The presence of two electron-donating phenylamino groups in the symmetric compound **1** makes this derivative easier to oxidize than the nonsymmetric compound **2** with its electronegative chlorine, hence the need to apply a higher potential (∼ 600 mV) for **2**.

UV−Vis Spectroscopy. Steady-state absorption and fluorescence emission spectra of **1** are depicted in Figure 4. Table 2 compiles the spectroscopic and photophysical data of **1** in
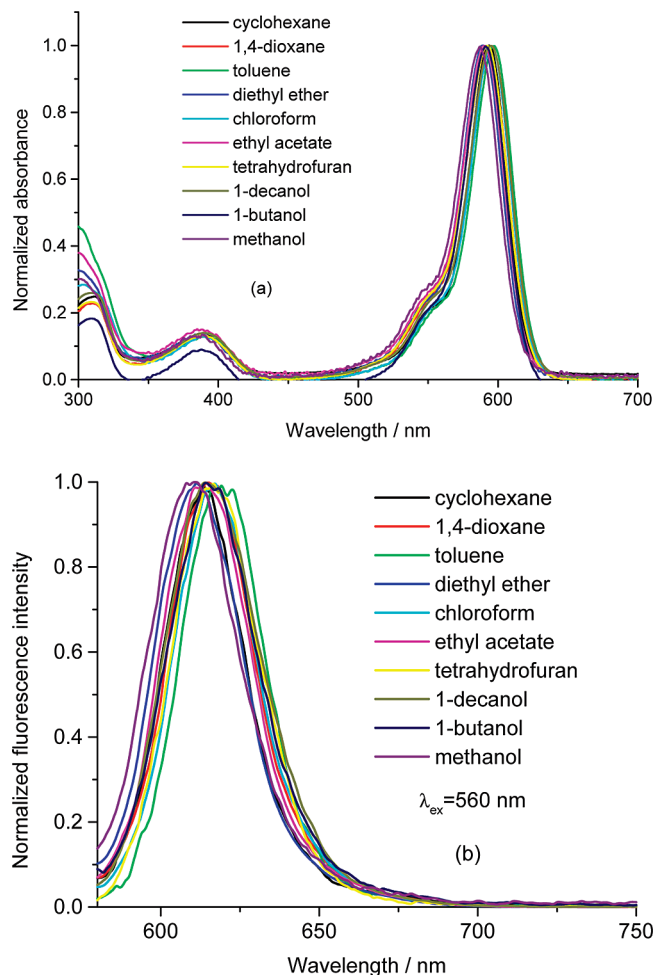
3,5-Dianilino Substituted Difluoroboron Dipyrromethene

J. Phys. Chem. C, Vol. 113, No. 27, 2009 **11735**

Figure 4. (a) Absorption spectra of **1** in different solvents normalized to 1.0. (b) Corresponding normalized fluorescence emission spectra (excitation at 560 nm).

the solvents used. The maximum absorption wavelength $\lambda_{abs}(max)$ of **1** is shifted to the red in comparison to the nonsymmetric dye **2**:[21] from 65 nm in cyclohexane (from 529 nm for **2** to 594 nm for **1**) to 90 nm in methanol (from 498 to 588 nm). The absorption spectra of **1** show the well-known absorption pattern of common BODIPY derivatives.[9,18] In all solvents tested, the main absorption band—attributed to the 0–0 vibrational band of a strong $S_0 \rightarrow S_1$ transition—is situated around 590 nm with a shoulder at the short wavelength side (at ~560 nm), assigned to the 0–1 vibrational band of the same transition. The $S_0 \rightarrow S_2$ transition is located around 375 nm. The $\lambda_{abs}(max)$ of the major absorption

band (i.e., around ~590 nm) is red-shifted with increasing polarizability of the solvent, from 588 nm in methanol to 597 nm in toluene. The fwhm$_{abs}$ of the main $S_0 \rightarrow S_1$ band of the symmetric compound **1** increases from 914 cm^{-1} in cyclohexane to 1062 cm^{-1} in 1,4-dioxane and THF, and it is always less than half that of the nonsymmetric dye **2** (e.g., the corresponding lower and upper fwhm$_{abs}$ values of **2** are 2545 cm^{-1} in cyclohexane and 3453 cm^{-1} in ethyl acetate). The fluorescence excitation spectra always match the absorption spectra and, furthermore, $\lambda_{abs}(max) = \lambda_{ex}(max)$.

The larger fwhm$_{abs}$ values observed for the absorption and fluorescence bands of **2** (which are anomalously large compared to those of most BOPDIPYs) have been discussed extensively in ref 21. They are due to the fact that **2** has a relative strong bond alternation in the ground state which changes upon excitation. In polar solvents there will be an additional contribution of solvent reorganization due to the change in dipole moment (size and orientation) upon excitation. This is typical "merocyanine" behavior because there is a significant net charge shift from the anilino moiety to the opposite five membered ring of BODIPY. Conversely, for **1** the major delocalized forms have a similar contribution in both the ground and excited states (as indicated by the small dipole moments in the ground and excited states). Hence, there is much less bond alternation and change thereof upon excitation.

The fluorescence emission spectra of **1** display narrow, slightly Stokes-shifted emission bands that are red-shifted by 44–49 nm compared to those of **2**. The $\lambda_{em}(max)$ are blue-shifted with decreasing polarizability of the solvent, from 620 nm in toluene to 611 nm in methanol.

Solvent-dependent spectral shifts are often interpreted in terms of the Lippert–Mataga equation (eq 4a), which describes the solvatochromic Stokes shift $\Delta\bar{\nu}$ (expressed in wavenumbers) as a function of the change of the dipole moment $\Delta\mu_{ge} = \mu_e - \mu_g$ of **1** upon excitation. The validity of eq 4a can be checked by using various solvents with different dielectric constants (ε) and refractive indices (n) and by plotting $\Delta\bar{\nu}$ as a function of $\Delta f = f(\varepsilon) - f(n^2)$.[30,31]

$$\Delta\bar{\nu} = \frac{2\Delta f}{4\pi\varepsilon_0 hca^3}(\mu_e - \mu_g)^2 + \text{constant} \qquad (4a)$$

$$f(\varepsilon) = (\varepsilon - 1)/(2\varepsilon + 1) \quad \text{and} \quad f(n^2) = (n^2 - 1)/(2n^2 + 1) \qquad (4b)$$

In eq 4a, $\Delta\bar{\nu} = \bar{\nu}_{abs} - \bar{\nu}_{em}$ is the solvatochromic shift (in cm^{-1}) between absorption [$\bar{\nu}_{abs} = 1/\lambda_{abs}(max)$] and fluores-

TABLE 2: Photophysical Data of Dye 1 in Several Solvents

	solvent[a]	SdP	λ_{abs}(max)/nm	λ_{em}(max/nm)	fwhm$_{abs}$/cm^{-1}	$\Delta\bar{\nu}$/cm^{-1}	Φ_f	τ^b/ns	k_f/10^8 s^{-1}	k_f/($n^2\,\bar{\nu}_{em}^3$)/10^{-5} s^{-1} cm^3	k_{nr}/10^8 s^{-1}
1	cyclohexane	0.000	594	613	914	522	0.86	4.01	2.1	2.2	0.4
2	1,4-dioxane	0.312	592	615	1062	632	0.66	3.61	1.8	1.9	0.9
3	toluene	0.284	597	620	988	621	0.61	3.72	1.6	1.6	1.0
4	diethyl ether	0.385	590	611	984	583	0.65	3.89	1.7	1.9	0.9
5	chloroform	0.614	595	617	964	599	0.79	4.01	2.0	2.0	0.5
6	ethyl acetate	0.603	590	614	1042	663	0.46	3.72	1.2	1.3	1.5
7	THF	0.634	593	617	1062	656	0.60	3.37	1.8	1.9	1.2
8	1-decanol	0.383	596	617	1051	571	0.73	4.03	1.8	1.9	0.7
9	1-butanol	0.655	593	614	978	577	0.63	3.74	1.7	1.8	1.0
10	methanol	0.904	588	611	1022	640	0.45	3.36	1.3	1.5	1.6

a The solvents are listed according to increasing polarity (as measured by the dielectric constant ε). *b* The standard errors on all lifetimes τ are ≤10 ps.

TABLE 3: Estimated Coefficients (y_0, a, b, c, d; see eq 5a), Their Standard Errors, and Correlation Coefficients (r) for the Multiple Linear Regression Analyses of $\bar{\nu}_{abs}$, $\bar{\nu}_{em}$, and $\Delta\bar{\nu}$ of 1 (Table 2) as a Function of the Kamlet−Taft (Eq 5b) and the New Catalán (Eq 5c) Solvent Scales

Kamlet−Taft	y_0 (cm^{-1})	a_α	b_β	c_{π^*}	r
$\bar{\nu}_{abs}$	$(16.83 \pm 0.09) \times 10^3$	-0.2 ± 1.1	1.1 ± 1.5	-0 ± 2	0.330
$\bar{\nu}_{em}$	$(16.32 \pm 0.07) \times 10^3$	0.3 ± 0.9	0.8 ± 1.3	-2.1 ± 1.4	0.566
$\Delta\bar{\nu}$	$(5.1 \pm 0.2) \times 10^2$	-0.5 ± 0.3	0.3 ± 0.4	2.0 ± 0.4	0.900

Catalán	y_0 (cm^{-1})	a_{SA}	b_{SB}	c_{SP}	d_{SdP}	r
$\bar{\nu}_{abs}$	$(17.7 \pm 0.2) \times 10^3$	-96 ± 92	-52 ± 56	$(-1.2 \pm 0.3) \times 10^3$	$(1.5 \pm 0.7) \times 10^2$	0.926
$\bar{\nu}_{abs}$	$(17.5 \pm 0.2) \times 10^3$			$(-1.0 \pm 0.2) \times 10^3$	86 ± 59	0.887
$\bar{\nu}_{em}$	$(17.2 \pm 0.2) \times 10^3$	30 ± 81	-56 ± 50	$(-1.2 \pm 0.2) \times 10^3$	-25 ± 63	0.933
$\Delta\bar{\nu}$	507 ± 176	-126 ± 82	5 ± 50	43 ± 235	172 ± 63	0.778

cence emission [$\bar{\nu}_{em} = 1/\lambda_{em}(max)$] maxima, and a represents the radius of the cavity in which the solute resides. μ_g and μ_e denote the dipole moments of **1** in the ground and excited states, respectively. The use of eq 4a is limited to transitions where the excited state reached after excitation is also the emissive state (hence, for $S_0 \rightarrow S_1$ excitation and equal dipole moments for the Franck−Condon and relaxed states) and where the excited-state dipole moment is independent of solvent polarity.

The Lippert−Mataga plot of the Stokes shift $\Delta\bar{\nu}$ versus Δf for **1** for the solvents of Table 2 is represented in Figure S2a (Supporting Information). There is a very poor linear relationship (correlation coefficient $r = 0.302$) between $\Delta\bar{\nu}$ and Δf in all solvents tested.

Mathematically, the solvent effect on $\bar{\nu}_{abs}$, $\bar{\nu}_{em}$, and $\Delta\bar{\nu}$ can also be formulated by a multilinear expression (eq 5a):

$$y = y_0 + aA + bB + cC + dD \qquad (5a)$$

where y denotes the solvent-dependent physicochemical property (here $\bar{\nu}_{abs}$, $\bar{\nu}_{em}$, $\Delta\bar{\nu}$) in a given solvent; y_0 is the value of this physicochemical property in the gas phase; and a, b, c, and d are adjustable regression coefficients that reflect the sensitivity of the physicochemical property y in a given solvent to the solvent properties A, B, C, and D. In the literature there are several solvent scales reported to describe the solvent dependence of y. Kamlet and Taft[32] proposed the π^*, α, and β parameters to characterize, respectively, the polarity/polarizability, the acidity, and the basicity of a solvent (eq 5b).

$$y = y_0 + a_\alpha\alpha + b_\beta\beta + c_{\pi^*}\pi^* \quad \text{(Kamlet − Taft)} \qquad (5b)$$

Recently, Catalán proposed a generalized treatment of the solvent effect based on a set of four empirical, mutually independent solvent scales.[33] SdP,[33] SP,[34] SA,[35,36] and SB[37] characterize the dipolarity, polarizability, acidity, and basicity, respectively, of a certain solvent (eq 5c).

$$y = y_0 + a_{SA}SA + b_{SB}SB + c_{SP}SP + \\ d_{SdP}SdP \quad \text{(Catalán, new)} \qquad (5c)$$

The Kamlet−Taft solvatochromic parameters α, β, and π^* are taken from ref 38, whereas the Catalán SA and SB parameters come from refs 35−37. The Catalán solvent polarizability parameters SP are collected from ref 34. The new SdP

solvent dipolarity parameters can be found in ref 33 and are also listed in Table 2.

Table 3 compiles the estimated regression coefficients y_0, a, b, c, and d (see eq 5a) and their respective standard errors, and the correlation coefficients (r) for the multiple linear regression analyses of the maxima of absorption ($\bar{\nu}_{abs}$) and fluorescence emission ($\bar{\nu}_{em}$) and the Stokes shift $\Delta\bar{\nu}$ of **1** according to eqs 5b and 5c for the solvents of Table 2. The analysis of the $\bar{\nu}_{abs}$ data according to Kamlet−Taft (eq 5b) using a solvent scale in which solvent polarity and polarizability effects are combined in the single parameter π^* shows a poor fit, as assessed by the value of r (0.330) and the large standard errors on the estimated parameters a_α, b_β, and c_{π^*} as quality-of-fit criteria. Conversely, use of the new Catalán solvent parameter set (eq 5c), where solvent (di)polarity and polarizability effects are split, gives an excellent multilinear fit to $\bar{\nu}_{abs}$ ($r = 0.926$). To visualize the goodness-of-fit of $\bar{\nu}_{abs}$ as a function of the Catalán solvent parameters {SA, SB, SP, SdP}, we made a graph (Figure 5a) of the absorption maxima $\bar{\nu}_{abs}$ calculated according to eq 5c using the estimated values of y_0, a_{SA}, b_{SB}, c_{SP}, and d_{SdP} versus the corresponding experimental $\bar{\nu}_{abs}$ values. As foreseen, an excellent linear relation ($r = 0.926$) is found with a slope close to unity (0.9 ± 0.1). From this plot, it is clear that 1,4-dioxane (#2) gives an outlier. The analysis of $\bar{\nu}_{abs}$ according to eq 5c without 1,4-dioxane gives a perfect fit ($r = 0.996$). Because the multiple linear regression of $\bar{\nu}_{abs}$ recovered relatively small estimates for a_{SA} and b_{SB} with comparatively large associated standard errors ($a_{SA} = -96 \pm 92$, $b_{SB} = -52 \pm 56$), we decided to perform the multilinear analysis with solvent dipolarity (SdP) and polarizability (SP) as the only solvent scales. This analysis (eq 5c with {SP, SdP} as independent variables) still gave a very good fit ($r = 0.887$), implying that solvent dipolarity and polarizability are the principal factors influencing the shifts of $\bar{\nu}_{abs}$.

For $\bar{\nu}_{em}$, the new Catalán (eq 5c) solvent scales produced definitely the best results ($r = 0.933$ for Catalán versus 0.566 for Kamlet−Taft). Figure 5b shows the linear relationship between the emission maxima $\bar{\nu}_{em}$ calculated according to eq 5c using the estimated values of y_0, a_{SA}, b_{SB}, c_{SP}, and d_{SdP} versus the corresponding experimental $\bar{\nu}_{em}$ values. Here also, an excellent linear relationship ($r = 0.933$) is found with a slope close to one (0.9 ± 0.1). The analysis according to eq 5c gave relatively small estimates for a_{SA}, b_{SB}, and c_{SdP} with correspondingly large standard errors. The fit according to eq 5c, which neglects solvent acidity and basicity, still gave a very good fit ($r = 0.915$ compared to $r = 0.933$ for the fit with {SA, SB, SdP, and SP} as independent variables). Hence, as for $\bar{\nu}_{abs}$, solvent acidity and basicity are not primarily responsible for the shift of $\bar{\nu}_{em}$.

3,5-Dianilino Substituted Difluoroboron Dipyrromethene
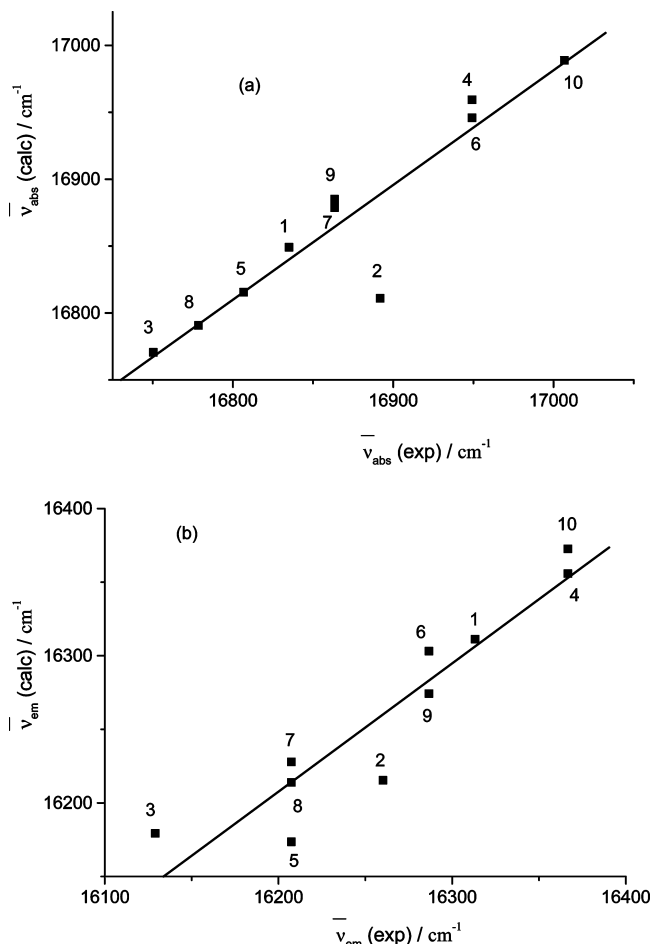
J. Phys. Chem. C, Vol. 113, No. 27, 2009 **11737**

Figure 5. (a) Linear relationship between the experimental and calculated $\bar{\nu}_{abs}$ of **1** obtained by the multiple linear regression analysis according to eq 5c in which y_0, a_{SA}, b_{SB}, c_{SP}, and d_{SdP} are the estimated regression coefficients. The numbers refer to the solvents of Table 2. The straight line is the best linear fit ($r = 0.926$, slope $= 0.9 \pm 0.1$) to the data. (b) Analogous linear relationship between $\bar{\nu}_{em}(calc)$ and $\bar{\nu}_{em}(exp)$ of **1**. The straight line is the best linear fit ($r = 0.933$, slope $= 0.9 \pm 0.1$) to the data.

In contrast to the poor linear relationships found in the plots of $\bar{\nu}_{abs}$ versus $f(n^2)$ ($r = 0.784$) and of $\bar{\nu}_{em}$ versus $f(n^2)$ ($r = 0.657$) obtained for BODIPY **2**,[21] the linearity of the plots for **1** (Figure S5, Supporting Information) of $\bar{\nu}_{abs}$ versus $f(n^2)$ ($r = 0.957$) and of $\bar{\nu}_{em}$ versus $f(n^2)$ ($r = 0.938$) confirms that van der Waals and excitonic interactions with a polarizable solvent are primarily responsible for the experimentally observed solvent-dependent shifts.[39] The slopes of the plots of $\bar{\nu}_{abs}$ [$(-4.7 \pm 0.5) \times 10^3$ cm^{-1}] and $\bar{\nu}_{em}$ [$(-4.2 \pm 0.5) \times 10^3$ cm^{-1}] versus $f(n^2)$ are similar. This agrees with our assumption that the Franck–Condon excited state and the relaxed, fluorescent excited state are virtually identical: they have the same oscillator strength and nearly the same energy. If a large difference in permanent dipole moment would exist between the ground and excited states, the excitation energy would depend linearly on the Lippert solvent parameter Δf rather than on $f(n^2)$ alone and hence no linear dependence on $f(n^2)$ would be observed anymore. Indeed, the plots (Figure S2, Supporting Information) of Stokes shifts $\Delta \bar{\nu}$ versus Δf, $\bar{\nu}_{abs}$ versus Δf, and $\bar{\nu}_{em}$ versus Δf display inadequate linear relationships, as judged by the r-values as quality-of-fit criteria ($r = 0.302$, 0.500, and 0.499 for $\Delta \bar{\nu}$, $\bar{\nu}_{abs}$, and $\bar{\nu}_{em}$, respectively). This indicates that both the emitting and absorbing states have a similar (and probably very small)

dipole moment which corresponds to the semiempirical calculations (Table 5).

Semiempirical calculations show that, upon replacing the chlorine by an anilino moiety at the 5-position, the Mulliken charge at the 6- and 7-positions becomes more negative by -0.03 and -0.015, respectively. In this respect, it is also interesting to compare the proton resonances of the anilino protons in **1** and **2**. Using the relation $\Delta \delta \approx 10 \Delta \rho$ (where ρ is the charge density on the carbons and δ the chemical shift of the hydrogens),[40] substitution of the chlorine atom at the 5-position with a phenylamino group changes the charge density by -0.016 at the 6-position and by -0.025 at the 7-position. For the 1- and 2-positions, the calculations show an increased negative charge density of -0.019 and -0.012, respectively. This does not correspond with the changes in the proton resonance, indicating a change by $+0.024$ and 0.0 at the 1- and 2-positions, respectively. The discrepancy between changes in charge density on the ring where no substitution occurs indicates that the chemical shifts are influenced not only by charges but also by an anisotropy effect. Increasing the electron density in the ring will increase the aromatic character and hence the ring current. The relative importance of the changes of ring current and charge density are probably not the same for both pyrrole rings in BODIPY.

Additionally, the resonances of the *ortho*-protons of the anilino moieties shift from 7.36 to 7.22 ppm upon introduction of the second anilino moiety (which corresponds to a change of -0.015 for the charge density on the *ortho*-carbons). This indicates that the electron donating effects of both anilino moieties are less than additive. Although introduction of the second anilino moiety increases the electron density in the BODIPY core, as indicated by the chemical shifts of the hydrogens of the pyrrole ring and the *meso*phenyl, it will probably not increase the ground-state dipole perpendicular to the long axis while the symmetric structure of **1** will exclude a component of a permanent dipole moment and bond alternation along the long axis in both the ground and the excited states. As even in apolar solvents the fwhm$_{abs}$ of **1** is reduced compared to the case of **2**, the changes in bond length upon excitation will be smaller in **1** compared to **2**. This is not surprising because **2** will have some extent of bond length alternation (which is inverted upon excitation) while this will not be the case for **1**.

The multilinear fit of the small Stokes shifts $\Delta \bar{\nu}$ according to Kamlet–Taft ($r = 0.900$) was better than that to Catalán ($r = 0.778$).

Because the SdP parameters were not available at the time of reporting the solvatochromic shifts of compound **2**,[21] it is appealing to perform the multilinear Kamlet–Taft and new Catalán analyses for the nonsymmetric derivative **2** as well. The absorption ($\bar{\nu}_{abs}$) and emission ($\bar{\nu}_{em}$) maxima and Stokes shifts ($\Delta \bar{\nu}$) of **2** as a function of the solvents used can be found in ref 21. Table 4 compiles the estimated regression coefficients y_0, a, b, c, and d and their respective standard errors, and the r-values for the multiple linear regression analyses of $\bar{\nu}_{abs}$, $\bar{\nu}_{em}$, and $\Delta \bar{\nu}$ of **2** according to eqs 5b and 5c for the solvents reported in ref 21. The most noticeable results are the much improved analyses of $\bar{\nu}_{abs}$ and $\bar{\nu}_{em}$ according to Kamlet–Taft obtained for **2** compared with **1**. The analyses according to Catalán, however, remain also for **2** superior to those according to Kamlet–Taft.

From the analyses of $\bar{\nu}_{abs}$ according to eqs 5b and 5c it is clear that solvent acidity is an irrelevant factor determining the position of $\bar{\nu}_{abs}$. Indeed, disregarding solvent acidity in eq 5b (Kamlet–Taft) gives an r-value (0.811) that is almost the same (0.818) as that for the multilinear regression of $\bar{\nu}_{abs}$ as a function

TABLE 4: Estimated Coefficients (y_0, a, b, c, d; See Eq 5a), Their Standard Errors, and Correlation Coefficients (r) for the Multiple Linear Regression Analyses of $\bar{\nu}_{abs}$, $\bar{\nu}_{em}$, and $\Delta\bar{\nu}$ of 2 (Ref 21) as a Function of the Kamlet−Taft (Eq 5b) and the New Catalán (Eq 5c) Solvent Scales

Kamlet−Taft	y_0 (cm^{-1})	a_α	b_β	c_{π^*}	r
$\bar{\nu}_{abs}$	$(18.9 \pm 0.3) \times 10^3$	-2 ± 3	10 ± 5	7 ± 5	0.818
$\bar{\nu}_{em}$	$(17.63 \pm 0.05) \times 10^3$	2.1 ± 0.6	-0.3 ± 0.8	-3.2 ± 0.9	0.909
$\Delta\bar{\nu}$	$(1.2 \pm 0.2) \times 10^3$	-4 ± 3	10 ± 4	10 ± 4	0.880

Catalán	y_0 (cm^{-1})	a_{SA}	b_{SB}	c_{SP}	d_{SdP}	r
$\bar{\nu}_{abs}$	$(20.2 \pm 0.9) \times 10^3$	-398 ± 439	491 ± 275	-1836 ± 1232	$(1.0 \pm 0.3) \times 10^3$	0.935
$\bar{\nu}_{em}$	$(18.2 \pm 0.2) \times 10^3$	347 ± 117	-91 ± 73	-875 ± 329	$(-1.7 \pm 0.9) \times 10^2$	0.921
$\Delta\bar{\nu}$	1965 ± 1053	-745 ± 499	582 ± 313	-961 ± 1402	$(1.2 \pm 0.4) \times 10^3$	0.915

TABLE 5: Calculated and Experimental Spectroscopic Properties for Molecules 1 and 2

	theory						experiment[a]			
E_{abs} (eV)	E_{emn} (eV)	Stokes shift (eV)	k_f (10^8 s^{-1})	state dipole S_0	state dipole S_1	ΔHOMO (eV)	E_{abs} (eV)	E_{emn} (eV)	Stokes shift (eV)[a]	k_f (10^8 s^{-1})[a]
1	2.21	2.15	0.06	1.9	4.24	1.6 (1.27)[b]	0.631	2.08	2	0.08	1.7
2	2.46	2.34	0.12	2.1	8.76	5.65 (5.84)[b]	1.143	2.37	2.16	0.21	2.6

[a] Toluene is taken as reference for experimental measurements. [b] The numbers in parentheses are the dipoles calculated for the relaxed excited-state geometry.

of $\{\alpha, \beta, \pi^*\}$. Similarly, the quality of the multiple linear fit of $\bar{\nu}_{abs}$ as a function of $\{SA, SB, SP, SdP\}$ (eq 5c, Catalán, $r = 0.935$) is only marginally better than that as a function of $\{SB, SP, SdP\}$ ($r = 0.921$).

The multilinear regressions of $\bar{\nu}_{em}$ according to Kamlet−Taft and Catalán both demonstrate that solvent basicity is the least significant factor for the position of $\bar{\nu}_{em}$ [as revealed by the comparatively small estimates for b_β (eq 5b) and b_{SB} (eq 5c) and their relatively large, corresponding standard errors]. Additional evidence comes from the analysis according to eq 5b with $\{\alpha, \pi^*\}$ as independent variables, which yields a fit with $r = 0.907$, comparable to the fit as a function of $\{\alpha, \beta, \pi^*\}$ ($r = 0.909$). This also is confirmed by the analysis according to eq 5c, in which solvent basicity is disregarded, which gives a fit with an r-value (0.889) close to that for the fit as a function of $\{SA, SB, SP, SdP\}$ ($r = 0.921$).

The multilinear fits of $\Delta\bar{\nu}$ according to Catalán ($r = 0.915$) and Kamlet−Taft ($r = 0.880$) are both of good quality. Fluorescence and absorption are shifted by the same amount by solvent polarizability, and hence their difference is independent of the SP parameter. Because there also is little change in dipole moment between the ground and excited states, there will be no shift of the absorption spectrum due to interaction with the permanent dipole moments of the solvent. Hence, the Stokes shift will also not show a systematic dependence on SdP.

In contrast to **2**,[21] the Φ_f values of **1** are much higher in all solvents used (ranging from 0.45 in methanol to 0.86 in cyclohexane). In the alcohol solvents, Φ_f increases along the series methanol < 1-butanol < 1-decanol.

Time-Resolved Fluorescence. Fluorescence decay histograms of **1** in different solvents were collected as a function of observation wavelength. The results of the time-resolved fluorescence measurements are also shown in Table 2. The fluorescence decays of **1** in all solvents could be described by monoexponential functions, $f(t) = \alpha \exp(-t/\tau)$. The lifetimes τ estimated via single curve analysis were independent of the observation wavelength, and global analysis confirmed the single-exponential nature of the decays with τ values on the nanosecond time scale. In the alcohol solvents, τ increases along the series methanol < 1-butanol < 1-decanol in accordance with the Φ_f values. The values of k_f, calculated according to eq 2a, are shown to be independent of the solvent

used [$k_f = (1.7 \pm 0.3) \times 10^8$ s^{-1}], similar to the (few) k_f values obtained for **2**.

Because k_f is proportional to the product of the squared transition dipole moment $|\mu|^2$, n^2, and $\bar{\nu}_{em}^3$ (eq 3), we calculated the ratio $k_f/(n^2 \bar{\nu}_{em}^3)$ of **1** for the solvents listed in Table 2 to check the solvent dependence of the transition dipole squared $|\mu|^2$. The multilinear regression of $k_f/(n^2 \bar{\nu}_{em}^3)$ according to Catalán (eq 5c with $\{SA, SB, SP, SdP\}$ as independent variables) gave an inadequate fit with $r = 0.554$, indicating that $k_f/(n^2 \bar{\nu}_{em}^3)$ is practically independent of the solvent. This implies that the transition dipole moment $|\mu|$ stays nearly constant in the solvents used.

The multilinear regression of k_{nr} of **1** for the solvents of Table 2 according to Catalán (eq 5c with $\{SA, SB, SP, SdP\}$ as independent variables) yielded a better fit, as assessed by $r = 0.765$. The linear regression of k_{nr} of **1** in the solvents of Table 2 as a function of SdP as a single independent variable yielded $r = 0.709$. The linear regressions of k_{nr} of **1** versus SA, SB, and SP gave inferior fits, as judged by the values of the corresponding correlation coefficients ($r = 0.418$, 0.359, and 0.467, respectively). This demonstrates that solvent polarity is the main factor determining the solvent-dependent trend of the rate constant for radiationless decay k_{nr} of BODIPY **1**. The plot of k_{nr} versus SdP (Figure S6, Supporting Information) shows an increase upon increasing solvent polarity, as observed for several BODIPY derivatives.

Quantum-Chemical Calculations. The spectroscopic properties of **1** (absorption and emission vertical transition energies), as computed for the isolated molecule at the INDO/SCI level, are collected in Table 5 together with the corresponding data previously reported for **2**.[21] The quantum-chemical calculations reproduce the overall trend observed experimentally upon substitution with one and two anilino moieties and yield a more quantitative description of the spectroscopic properties, namely of the Stokes shift, in the case of **1**. The origin of the bathochromic displacement observed when going from **1** to **2** is unambiguously associated with an extension of the π-system through the second anilino arm, as illustrated by the transition density maps of the lowest electronic excitations in Figure 6. The computed radiative decay rate constants for molecules **1** and **2** are comparable yet slightly larger for **2**. This might seem
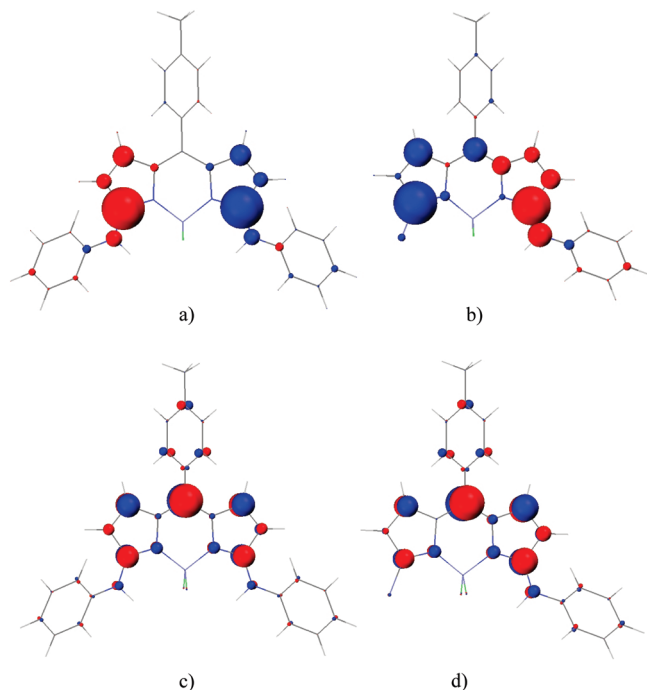
3,5-Dianilino Substituted Difluoroboron Dipyrromethene

J. Phys. Chem. C, Vol. 113, No. 27, 2009 **11739**

Figure 6. Transition density distributions calculated at the INDO/SCI level for the lowest optical transition of **1** (a) and **2** (b). The blue spheres depict negative charges while red spheres indicate the presence of a positive charge. Shape of the HOMO orbital in **1** (c) and **2** (d). The blue atomic orbitals depict negative LCAO coefficients while the red atomic orbitals depict positive LCAO coefficients.

at odds with the increased π-delocalization in the bis-substituted BODIPY derivative **1** but can be easily explained by the fact that the higher excitation energy in **2** is accompanied by a lower transition dipole moment (owing to the redistributed transition densities, Figure 6), so that the two effects almost cancel out and result in a slightly smaller value for k_f of **1**. Note that similar k_f-values have been measured for **1** and **2**, with a slightly smaller value for **1** in toluene in accord with the quantum-chemical results.

The INDO/SCI state dipoles in the ground state and in the lowest excited state of **1** are, as expected, significantly smaller than those in **2**[21] and entirely oriented along the short axis of the molecule. The changes in state dipole upon photoexcitation suggest a (mild) negative dipolar solvatochromic effect (especially for the absorption spectrum) as in the nonsymmetric dye **2**[21] (the ground-state dipole is larger than the excited-state dipole so that the absorption spectrum should blue shift with increasing solvent polarity). As described above, the solvatochromic effects observed for **1** are small and mostly governed by the solvent polarizability.

The one-electron energy diagrams computed for **1** and **2** in comparison to the reference compound **3** (BODIPY substituted by chlorine atoms at the 3,5-positions) show that substitution of chlorine atoms with anilino electron-donating moieties leads to a destabilization of the HOMO level, in good agreement with the lower oxidation potential found for **1** (see also Figure 6).

Conclusions

A symmetric, 3,5-diphenylamino-substituted difluoroboron dipyrromethene dye (**1**) has been synthesized by nucleophilic substitution of 3,5-dichloroBODIPY **3** with aniline. The solvent-dependent photophysical properties have been investigated by means of UV−vis spectrophotometry and steady-state and time-resolved fluorometry. Our study demonstrates the large effect

of the phenylamino substituent on the fluorescence characteristics of the dye. The symmetric dye **1** has higher quantum yields Φ_f (0.45−0.86) and longer fluorescence lifetimes τ (3.36− 4.03 ns) in all solvents studied compared to those of **2**. The emission maxima λ_{em}(max) of **1** are shifted to the red by ∼45 nm in comparison to those of the nonsymmetrically substituted derivative **2**. The fwhm$_{abs}$ and Stokes shifts $\Delta\bar{\nu}$ of symmetric **1** are much smaller than those for nonsymmetric **2**. For both dyes, the value of the fluorescence rate constant [$k_f = (1.7 \pm 0.3) \times 10^8$ s^{-1}] does not vary much between the solvents studied. A large difference is evident in the redox electrochemistry of the two dyes, with the symmetric compound **1** possessing a much lower oxidation potential (∼600 mV) in comparison to the nonsymmetric system **2**. This can be ascribed to the presence of two electron-donating phenylamino groups in **1**, which increases the electron density in the conjugated chain and hence facilitates oxidation compared to the nonsymmetric compound **2** with its electron-withdrawing chlorine. The crystal structure of **1** shows that the BODIPY core is planar and that the *meso*-substituent is almost perpendicular to it. Quantum-chemical calculations corroborate the different photophysical behaviors of the symmetric and nonsymmetric derivatives.

Supporting Information Available: Table with hydrogen bond distances and angles in the dimeric structure of **1**. Figure displaying the aggregation of **1** through a series of hydrogen bonds and $\pi-\pi$ stacking interactions in the crystal cell. Plots of the absorption and emission maxima of **1** versus SP and SdP. Plots of the Stokes shifts, the absorption maxima, and the emission maxima of **1** versus the Lippert solvent parameter Δf. 600 MHz ^{1}H NMR and 150 MHz ^{13}C NMR of compound **1**. This material is available free of charge via the Internet at http://pubs.acs.org.

References and Notes

(1) Treibs, A.; Kreuzer, F.-H. *Liebigs Ann. Chem.* **1968**, *718*, 208–223.

(2) (a) Loudet, A.; Burgess, K. *Chem. Rev.* **2007**, *107*, 4891–4932. (b) Ulrich, G.; Ziessel, R.; Harriman, A. *Angew. Chem., Int. Ed.* **2008**, *47*, 1184–1201.

(3) Haugland, R. P. *The Handbook. A Guide to Fluorescent Probes and Labeling Technologies*, 10th ed.; Molecular Probes, Inc.: Eugene, Oregon, 2005.

(4) (a) Karolin, J.; Johansson, L. B.-Å.; Strandberg, L.; Ny, T. *J. Am. Chem. Soc.* **1994**, *116*, 7801–7806. (b) Bergström, F.; Mikhalyov, I.; Hägglöf, P.; Wortmann, R.; Ny, T.; Johansson, L. B.-Å. *J. Am. Chem. Soc.* **2002**, *124*, 196–204. (c) Gabe, Y.; Urano, Y.; Kikuchi, K.; Kojima, H.; Nagano, T. *J. Am. Chem. Soc.* **2004**, *126*, 3357–3367. (d) Basarić, N.; Baruah, M.; Qin, W.; Metten, B.; Smet, M.; Dehaen, W.; Boens, N. *Org.*

11740 *J. Phys. Chem. C, Vol. 113, No. 27, 2009*

Qin et al.

Biomol. Chem. **2005**, *3*, 2755–2761. (e) Yamada, K.; Nomura, Y.; Citterio, D.; Iwasawa, N.; Suzuki, K. *J. Am. Chem. Soc.* **2005**, *127*, 6956–6957. (f) Malval, J.-P.; Leray, I.; Valeur, B. *New J. Chem.* **2005**, *29*, 1089–1094. (g) Coskun, A.; Akkaya, E. U. *J. Am. Chem. Soc.* **2005**, *127*, 10464–10465. (h) Wu, Y.; Peng, X.; Guo, B.; Fan, J.; Zhang, Z.; Wang, J.; Cui, A.; Gao, Y. *Org. Biomol. Chem.* **2005**, *3*, 1387–1392. (i) Mei, Y.; Bentley, P. A.; Wang, W. *Tetrahedron Lett.* **2006**, *47*, 2447–2449. (j) Kim, H. J.; Kim, J. S. *Tetrahedron Lett.* **2006**, *47*, 7051–7055. (k) Qi, X.; Jun, E. J.; Xu, L.; Kim, S. J.; Hong, J. S. J.; Yoon, Y. J.; Yoon, J. *J. Org. Chem.* **2006**, *71*, 2881–2884. (l) Peng, X.; Du, J.; Fan, J.; Wang, J.; Wu, Y.; Zhao, J.; Sun, S.; Xu, T. *J. Am. Chem. Soc.* **2007**, *129*, 1500–1501.

(5) Thoresen, L. H.; Kim, H.; Welch, M. B.; Burghart, A.; Burgess, K. *Synlett* **1998**, 1276.

(6) Ulrich, G.; Ziessel, R. *J. Org. Chem.* **2004**, *69*, 2070–2083.

(7) Goud, T. V.; Tutar, A.; Biellmann, J. F. *Tetrahedron* **2006**, *62*, 5084–5091.

(8) Baruah, M.; Qin, W.; Basarić, N.; De Borggraeve, W. M.; Boens, N. *J. Org. Chem.* **2005**, *70*, 4152–4157.

(9) (a) Qin, W.; Baruah, M.; Van der Auweraer, M.; De Schryver, F. C.; Boens, N. *J. Phys. Chem. A* **2005**, *109*, 7371–7384. (b) Qin, W.; Baruah, M.; Stefan, A.; Van der Auweraer, M.; Boens, N. *ChemPhysChem* **2005**, *6*, 2343–2351.

(10) Baruah, M.; Qin, W.; Vallée, R. A. L.; Beljonne, D.; Rohand, T.; Dehaen, W.; Boens, N. *Org. Lett.* **2005**, *7*, 4377–4380.

(11) Rohand, T.; Baruah, M.; Qin, W.; Boens, N.; Dehaen, W. *Chem. Commun.* **2006**, 266–268.

(12) Rohand, T.; Qin, W.; Boens, N.; Dehaen, W. *Eur. J. Org. Chem.* **2006**, 4658–4663.

(13) Qin, W.; Rohand, T.; Baruah, M.; Stefan, A.; Van der Auweraer, M.; Dehaen, W.; Boens, N. *Chem. Phys. Lett.* **2006**, *420*, 562–568.

(14) Qin, W.; Rohand, T.; Dehaen, W.; Clifford, J. N.; Driessen, K.; Beljonne, D.; Van Averbeke, B.; Van der Auweraer, M.; Boens, N. *J. Phys. Chem. A* **2007**, *111*, 8588–8597.

(15) Rohand, T.; Lycoops, J.; Smout, S.; Braeken, E.; Sliwa, M.; Van der Auweraer, M.; Dehaen, W.; De Borggraeve, W. M.; Boens, N. *Photochem. Photobiol. Sci.* **2007**, *6*, 1061–1066.

(16) Qin, W.; Baruah, M.; Sliwa, M.; Van der Auweraer, M.; De Borggraeve, W. M.; Beljonne, D.; Van Averbeke, B.; Boens, N. *J. Phys. Chem. A* **2008**, *112*, 6104–6114.

(17) Baruah, M.; Qin, W.; Flors, C.; Hofkens, J.; Vallée, R. A. L.; Beljonne, D.; Van der Auweraer, M.; De Borggraeve, W. M.; Boens, N. *J. Phys. Chem. A* **2006**, *110*, 5998–6009.

(18) The following represents a nonexhaustive list of BODIPY papers with spectroscopic/photophysical data. (a) Vos de Wael, E.; Pardoen, J. A.; van Koeveringe, J. A.; Lugtenburg, J. *Recl. Trav. Chim. Pays-Bas* **1977**, *96*, 306–309. (b) Kollmannsberger, M.; Rurack, K.; Resch-Genger, U.; Daub, J. *J. Phys. Chem. A* **1998**, *102*, 10211–10220. (c) López Arbeloa, T.; López Arbeloa, F.; López Arbeloa, I.; García-Moreno, I.; Costela, A.; Sastre, R.; Amat-Guerri, F. *Chem. Phys. Lett.* **1999**, *299*, 315–321. (d) Rurack, K.; Kollmannsberger, M.; Daub, J. *New J. Chem.* **2001**, *25*, 289–292. (e) Rurack, K.; Kollmannsberger, M.; Daub, J. *Angew. Chem., Int. Ed.* **2001**, *40*, 385–387. (f) Costela, A.; García-Moreno, I.; Gomez, C.; Sastre, R.; Amat-Guerri, F.; Liras, M.; Lüpez Arbeloa, F.; Bañuelos Prieto, J.; Lüpez Arbeloa, I. *J. Phys. Chem. A* **2002**, *106*, 7736–7742. (g) Lüpez Arbeloa, F.; Bañuelos Prieto, J.; Martínez Martínez, V.; Arbeloa Lüpez, T.; Lüpez Arbeloa, I. *Chem. Phys. Chem.* **2004**, *5*, 1762–1771. (h) Bañuelos Prieto, J.; Lüpez Arbeloa, F.; Martínez Martínez, V.; Arbeloa Lüpez, T.; Amat-Guerri, F.; Liras, M.; Lüpez Arbeloa, I. *Chem. Phys. Lett.* **2004**, *385*, 29–35. (i) Qin, W.; Baruah, M.; De Borggraeve, W. M.; Boens, N. *J. Photochem. Photobiol. A: Chem.* **2006**, *183*, 190–197. (j) Dost, Z.; Atilgan, S.; Akkaya, E. U. *Tetrahedron* **2006**, *62*, 8484–8488. (k) Li, Z.; Bittman, R. *J. Org. Chem.* **2007**, *72*, 8376–8382. (l) Ekmekci, Z.; Yilmaz, M. D.; Akkaya, E. U. *Org. Lett.* **2008**, *10*, 461–464. (m) Li, L.; Han, J.; Nguyen, B.; Burgess, K. *J. Org. Chem.* **2008**, *73*, 1963–1970.

(19) Dilek, ö.; Bane, S. L. *Tetrahedron Lett.* **2008**, *49*, 1413–1416.

(20) Li, L.; Nguyen, B.; Burgess, K. *Bioorg. Med. Chem. Lett.* **2008**, *18*, 3112–3116.

(21) Qin, W.; Leen, V.; Rohand, T.; Dehaen, W.; Dedecker, P.; Van der Auweraer, M.; Robeyns, K.; Van Meervelt, L.; Beljonne, D.; Van Averbeke, B.; Clifford, J. N.; Driesen, K.; Binnemans, K.; Boens, N. *J. Phys. Chem. A* **2009**, *113*, 439–447.

(22) Sheldrick, G. M. *SHELXS97 Program for Solution of Crystal Structure*; University of Göttingen: Germany, 1997.

(23) Olmsted, J. *J. Phys. Chem.* **1979**, *83*, 2581–2584.

(24) Valeur, B. *Molecular Fluorescence. Principles and Applications*; Wiley-VCH: Weinheim, Germany, 2002.

(25) (a) O'Connor, D. V.; Phillips, D. *Time-correlated Single Photon Counting*; Academic Press: New York, 1984. (b) vandeVen, M.; Ameloot, M.; Valeur, B.; Boens, N. *J. Fluoresc.* **2005**, *15*, 377–413. (c) Boens, N.; Qin, W.; Basarić, N.; Hofkens, J.; Ameloot, M.; Pouget, J.; Lefèvre, J.-P.; Valeur, B.; Gratton, E.; vandeVen, M.; Silva, N. D.; Engelborghs, Y.; Willaert, K.; Sillen, A.; Rumbles, G.; Phillips, D.; Visser, A. J. W. G.; Van Hoek, A.; Lakowicz, J. R.; Malak, H.; Gryczynski, I.; Szabo, A. G.; Krajcarski, D. T.; Tamai, N.; Miura, A. *Anal. Chem.* **2007**, *79*, 2137–2149.

(26) Crovetto, L.; Orte, A.; Talavera, E. M.; Alvarez-Pez, J. M.; Cotlet, M.; Thielemans, J.; De Schryver, F. C.; N. Boens, N. *J. Phys. Chem. B* **2004**, *108*, 6082–6092.

(27) Van den Zegel, M.; Boens, N.; Daems, D.; De Schryver, F. C. *Chem. Phys.* **1986**, *101*, 311–335.

(28) Dewar, M. J. S.; Zoebisch, E. G.; Healy, E. F.; Stewart, J. J. P. *J. Am. Chem. Soc.* **1985**, *107*, 3902–3909.

(29) Zerner, M. C. In *Reviews in Computational Chemistry*; Lipkowitz, K. W., Boyd, D. B., Eds.; VCH: New York, 1991; Vol. 2, pp 313–365.

(30) Lippert, E. Z. *Naturforsch. A: Phys. Sci.* **1955**, *10*, 541–545.

(31) Mataga, N.; Kaifu, Y.; Koizumi, M. *Bull. Chem. Soc. Jpn.* **1955**, *28*, 690–691; **1956**, *29*, 465–470.

(32) Kamlet, M. J.; Taft, R. W. *J. Am. Chem. Soc.* **1976**, *98*, 377–383.

(33) Catalán, J. *J. Phys. Chem. B* **2009**, *113*, 5951–5960.

(34) Catalán, J.; Hopf, H. *Eur. J. Org. Chem.* **2004**, 4694–4702.

(35) Catalán, J. In *Handbook of solvents*; Wypych, G., Ed.; ChemTec Publishing: Toronto, 2001; pp 583–616.

(36) Catalán, J.; Díaz, C. *Liebigs Ann.* **1997**, 1941–1949.

(37) Catalán, J.; Díaz, C.; López, V.; Pérez, P.; de Paz, J. L. G.; Rodriguez, J. G. *Liebigs Ann.* **1996**, 1785–1794.

(38) Marcus, Y. *Chem. Soc. Rev.* **1993**, *22*, 409–416.

(39) Pevenage, D.; Corens, D.; Dehaen, W.; Van der Auweraer, M.; De Schryver, F. C. *Bull. Soc. Chim. Belg.* **1997**, *106*, 565–572.

(40) Günther, H. *NMR spectroscopy*; John Wiley and Sons: Chichester, 1980, pp 68–69.